Intended for

Denka Performance Elastomer LLC, Request for Correction

Exhibit A

Date

July 15, 2021

SUPPLEMENTAL MATERIALS F
REACTIVE METABOLITE MODELING

Enhancing the PBPK Model for Chloroprene to include reactive oxidative metabolites responsible for the pulmonary toxicity and carcinogenicity

1. INTRODUCTION

A PBPK model was developed for chloroprene (CP; 2-chloro-1,3-butadiene) to estimate lung dose metrics and correlate these dose metrics with toxicity and carcinogenicity in the mouse (Clewell et al. 2019, 2020). The dose metric calculated with this PBPK model was total amount of chloroprene metabolized per gram of lung. Metabolism of chloroprene starts with oxidation via cytochrome P-450 enzymes producing two oxiranes – (1-chloroethenyl)oxirane (1-CEO) and (2-chloroethenyl)oxirane (2-CEO). Oxiranes produced by microsomal oxidation of ethenes, such as ethylene oxide or butadiene monoxide and butadiene diepoxide, are sufficiently stable to undergo Phase II metabolism by epoxide hydrolases (EHs) and glutathione transferases (GSTs) and to diffuse from the tissues where they are produced into the bloodstream for transport to other tissues (Johanson and Filser 1993; Kohn and Melnick 2000; Filser and Klein 2018). The goal of this present effort was to extend the PBPK model for chloroprene to include more detail on the epoxides and other reactive products formed by oxidative metabolism, and to describe the impact of production of reactive products on tissue glutathione (GSH).

In extending the PBPK model to include the production of various reactive intermediates, we examined papers on in vitro metabolism and analytical chemistry for identification of various metabolites of chloroprene (Cottrell et al. 2001; Munter et al. 2003; Himmelstein et al. 2004; Munter et al. 2007). Of the two reaction products formed by the microsomal oxidation of chloroprene, (1-chloroethenyl)oxirane (1-CEO) is expected to have a short, but measurable half-life in tissues. (2-chloroethenyl)oxirane, on the other hand, is expected to quickly rearrange to reactive aldehydes and ketones produced by both the spontaneous rearrangement of 2-CEO and the spontaneous rearrangement of the diepoxide and diepoxide diol produced from further oxidation of 1-CEO in the mouse (Himmelstein et al. 2004). This is similar to what has been observed with 1,1-DCE. The products of 2-CEO rearrangement are expected to react non-enzymatically and rapidly with GSH. The depletion of GSH by these aldehydes and ketones will affect the cellular GSH available for their detoxification. As GSH levels fall, the concentration of reactive metabolites increases, leading to exacerbation of toxic responses in the tissue because aldehydes and ketones then react with cellular constituents other than GSH. The expectations of increased tissue toxicity with GSH depletion are consistent with observations of liver and lung responses of fasted rats to CP inhalation (Jaeger et al. 1975; Plugge and Jaeger 1979) and similar responses in livers in fasted rats exposed to 1,1-DCE (McKenna et al. 1977; Andersen et al. 1980).

2. METHODS

Formation and clearance processes with 1-CEO: 1-CEO is formed by the oxidation of CP by cytochrome P450 enzymes, primarily CYP2f1 and 2e1 (Figure 1A). This oxidation step produces both 1- and 2-CEO and the relative split for the flux through both pathways was estimated separately for liver and lung microsomes (Himmelstein et al. 2004). In the subsequent equations, alpha (a) is the proportion of CYP-oxidation producing 1-CEO, and (1-a) is the

proportion producing 2-CEO (Figure 1A). In addition, the products of the first oxidation step include both the respective epoxide and diol due to the proximity of the cytochrome P450s and microsomal epoxide hydrolases within the microsomes, i.e. within the endoplasmic reticulum in the intact tissues. Thus, some diol is produced by an intracellular first-pass-like process where the proximity of the CYP enzymes and epoxide hydrolase in microsomal vesicles allows some direct conversion of the epoxide to the diol before release from the lipophilic environment of the microsome to the cytoplasm (Johanson and Filser 1993; Kohn and Melnick 2000). An estimate of the proportion of diol produced by the oxidation (b) was available from modeling with butadiene (Campbell et al. 2015). The subsequent clearance of 1-CEO occurs by three pathways in the mouse, EH/H2O hydrolysis, further microsomal oxidation of 1-CEO (Himmelstein et al. 2004) and, *in vivo*, diffusion of 1-CEO from tissue into the bloodstream. While reactions of 1-CEO with GSH, either catalyzed by GSTs or by direct non-enzymatic conjugation, are possible, there was no evidence for this pathway in human, rat, or mouse microsomal incubations (Munter et al. 2003). With human microsomes, there was no evidence of a second oxidation step consuming the 1-CEO (Himmelstein et al. 2004).

Kinetic constants for CP oxidation were estimated from in vitro studies following the loss of headspace CP from vials containing microsomal suspensions. Those for 1-CEO oxidation followed 1-CEO headspace loss using microsomal suspensions with added NADPH. 1-CEO hydrolysis was also assessed using microsomal preparations with no added NADPH. In these detailed kinetic studies of multiple pathways (Himmelstein et al. 2004), GSH conjugation was examined by evaluating loss of headspace 1-CEO with vials containing cytoplasm and 10 mM GSH – a GSH level about 5 times higher than background levels in lung (Csanady et al. 2003; Jaeger et al. 1974a). As noted in studies identifying metabolites of CP (Munter et al. 2003), there was no evidence for appreciable clearance of 1-CEO by reactions involving glutathione.

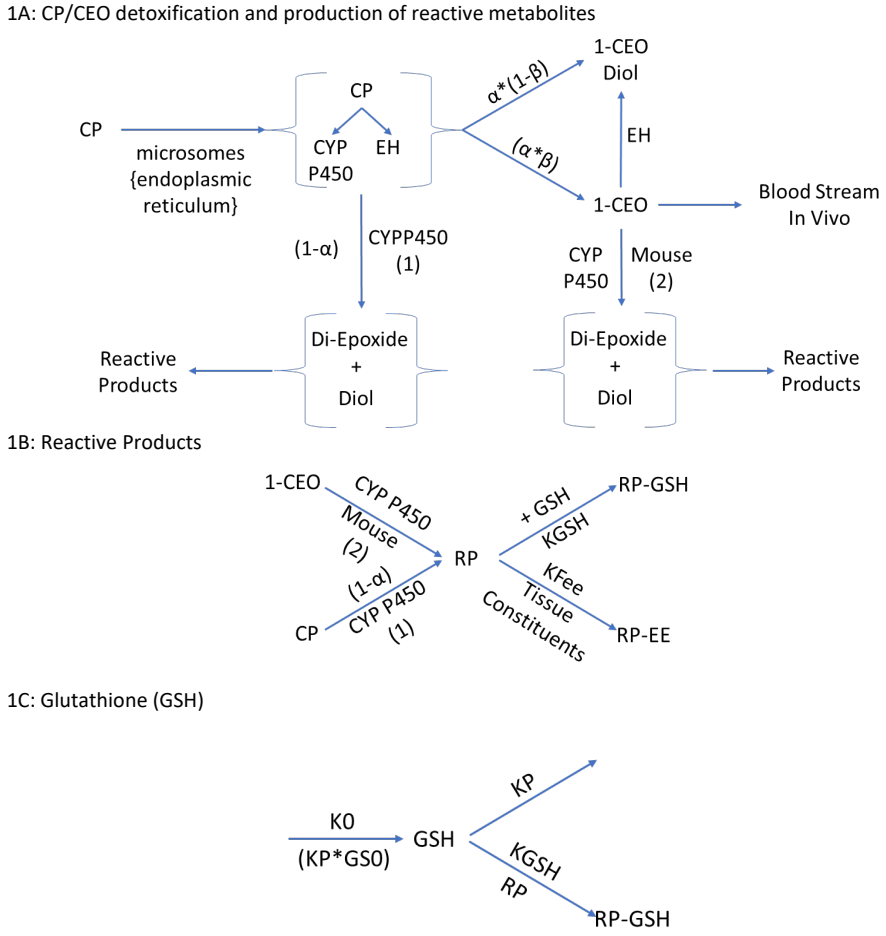

Figure F1. Schematics for the production and clearance of the three key components in the enhanced PBPK model for chloroprene (CP).

Formation and clearance processes with 2-CEO: In a fashion similar to 1-CEO, 2-CEO would be an intermediate of the oxidation of CP by CYP2e1 and 2f1 (Figure F1A). The proportion of 2-CEO formed is (1-α) times the net rate of loss of CP, where a is the proportion of the initial oxidation step that goes to 1-CEO. As with the formation of 1-CEO and 1-CEO diol, the proportion of the formation of the diol would be b times the total oxidation rate. However, neither 2-CEO nor 2-CEO diol are stable and they undergo rapid rearrangement to reactive aldehydes and ketones, all of which would react with GSH. Modeling of conjugation of reactive products with glutathione was similar to that used in PBPK models for reactive products with vinyl chloride (Clewell et al. 2001) and vinylidene chloride (D'Souza et al. 1988). In addition, the oxidative reaction of 1-CEO to a diepoxide also produces various reactive aldehydes and ketones. The net flux of all these reactive intermediates is captured in a single lumped compartment, called reactive products (RP).

Formation and tissue clearance of transient reactive products (RPs): The RP pool represents a group of reactive aldehydes and ketones that form by rearrangement of the unstable epoxide, 2-CEO, and of the diepoxide formed by oxidation of 1-CEO (Figure F2B). These products themselves are expected to be short-lived and react with other cellular components and with GSH, where the GSH conjugation pathway is favored at normal GSH concentrations. The rate

equation for RP would have the net rates of production of 2-CEO and the 1-CEO diepoxide and loss due to reaction with GSH and with other cellular constituents. The abbreviation, kfee, represent a first order rate constant for reaction of RP with "everything else". A first-order constant is used because the reaction of RP with these other tissue components is not expected to deplete the total reactant pool of these constituents to any great extent. A similar approach for modeling reactive intermediates was used with vinyl chloride (Clewell et al. 2001).

Depletion of GSH: The last process that needed to be included in the model was the production and removal of RP and the effect of higher rates of formation of RPs on GSH (Figure F1C). Higher rates of formation of RPs will cause depletion of GSH leading to increased tissue toxicity from these RPs. The rate constants for glutathione synthesis (Ko) and background loss (k1) have been approximated in various previous publications with vinyl chloride, ethylene dichloride and vinylidene chloride (D'Souza and Andersen 1988; D'Souza et al. 1988) and specifically for mouse lung in work with styrene and styrene oxide (Csanady et al. 2003). With these compounds, there is depletion of tissue glutathione, usually measured in liver, at higher exposures. While no direct measurements have been reported for GSH depletion in lungs caused by CP inhalation, the most sensitive gene ontology pathways affected by CP exposures in mice were associated with Nrf2-regulation of oxidative stress and GSH metabolism pathways (Thomas et al. 2013), an observation consistent with GSH loss during CP exposures.

Table F1. Parameters for the chloroprene metabolite model (chemical specific parameters for the physiology and chloroprene chemical specific parameters are reported in Supp Mat A).

Parameter	Description	Female Mouse	Female Rat
Chloroprene			
ALPHAL	Fraction of oxidative metabolism to 1-CEO in liver (remainder to 2-CEO)	0.02[1]	0.05[1]
ALPHALU	Fraction of oxidative metabolism to 1-CEO in lung (remainder to 2-CEO)	0.03[1]	0.15[1]
Fraction of total CP to 1-CEO privileged access			
BETA	Fraction of 1-CEO production available for hydrolysis/oxidative metabolism or release to blood	0.33[2]	0.33[2]
1-CEO			
Metabolism in Liver - Hydrolysis			
VMAXC1	Scaled VMax for Hydrolysis Pathway:Liver (mg/h/BW^0.75)	10.65[1]	62.1[1]
KM1	Km for Hydrolysis Pathway:Liver (mg/L)	1.9[1]	3.7[1]
Metabolism in Lung - Hydrolysis			
VMAXCLU1	Scaled VMax for Hydrolysis Pathway:Lung (mg/h/BW^0.75)	0.64[1]	0.85[1]
KMLU1	Km for Hydrolysis Pathway:Lung (mg/L)	4.6[1]	8.0[1]

Table F1. Parameters for the chloroprene metabolite model (chemical specific parameters for the physiology and chloroprene chemical specific parameters are reported in Supp Mat A).			
Parameter	**Description**	**Female Mouse**	**Female Rat**
Metabolism in Liver - Oxidative (Mouse pathway only)			
VMAXC1O	Scaled VMax for oxidative pathway in liver (mg/h/BW^0.75)	2.25[1]	NA
KM1O	Km for oxidative pathway in liver (mg/L)	1.5[1]	NA
LLOXACT	Lung to liver ratio for oxidative metabolism of 1-CEO (VMAXC10 scaled to lung)	0.42[4]	NA
Reactive Products			
K2LC	2nd order rate of RP reaction with GSH (L/umol/hr)	0.13[3]	0.13[3]
K2LUC	2nd order rate of RP reaction with GSH (L/umol/hr)	0.13[3]	0.13[3]
KFEEC	Conjugation rate with non-GSH (L/umol/hr)	35[3]	35[3]
LLEEACT	Lung to liver ratio for reactive products reaction with other cellular molecules (KFEEC scaled to lung)	0.14[4]	0.06[4]
GSH Parameters from ECD model			
KPC	First-order rate constant for GSH loss (/hr*kg $BW^{-0.3}$)	0.06[4]	0.06[4]
GSO	Initial GSH concentration in liver (uM)	7000[4]	5500[4]
GSOLU	Initial GSH concentration in lung (uM)	1500[4]	1200[4]
1-CEO Partition Coefficients			
PB1	Blood:Air	5.74[5]	5.74[5]
PLU1	Lung:Blood	0.69[5]	0.69[5]
PL1	Liver:Blood	1.18[5]	1.18[5]
PF1	Fat:Blood	5.15[5]	5.15[5]
PS1	Slowly Perfused:Blood	0.69[5]	0.69[5]
PR1	Rapidly Perfused:Blood	1.18[5]	1.18[5]

[1] Himmelstein et al. 2004

[2] Campbell et al. 2015

[3] Clewell et al. 2001

[4] Environ International 2004

[5] 1-CEO tissue:air and tissue:blood partitions were estimated using IndusChemFate (version 2.00, http://cefic-lri.org/toolbox/induschemfate/) and a logKow of 1.22 (KOWIN v.1.67 reported on Chemspider 2021. http://www.chemspider.com/Chemical-Structure.201536.html)

Metabolite Model Parameterization: The rate equations for the three components of the expanded model, i.e. 1-CEO (2A), RP (2B) and GSH (2C) are in Figure F2. The parameters used

in the chloroprene metabolite submodel are shown in Table F1 (IVIVE scaling of *in vitro* derived rate constants was performed in the same manner as in the parent chemical model). The fraction of total chloroprene metabolism to 1-CEO in liver (ALPHAL) and lung (ALPHALU) was reported in Himmelstein et al. (2004) for female mouse and rat. The fraction of 1-CEO that is available for distribution, hydrolysis, or oxidative metabolism (BETA) was set equal to the ratio for epoxybutene (Campbell et al. 2015) where 67% of the amount of epoxybutene produced from the metabolism of butadiene was further metabolized due to co-localization of enzymes (i.e. CYP P450 and EH) in the endoplasmic reticulum. The in vitro derived parameters for the hydrolysis and oxidative (mouse only) metabolism of 1-CEO in liver and lung were reported in Himmelstein et al. (2004). For the oxidative pathway in mouse, only the male mouse liver incubations provided levels of metabolism that allowed for estimation of the 1-CEO saturable metabolism parameters. The oxidative metabolism of 1-CEO in the lung was not measurable. As oxidative metabolism of 1-CEO could not be measured in the lung, the scaled liver maximum rate (VMAX1O) for the mouse was based on the ratio of the mixed function oxidase scaled in lung/liver (LLOXACT) previously reported for the mouse (Environ International 2004). The chemical reaction rate constants for the RP including the second order reaction with GSH in liver (K2L) and lung (K2LU), and reaction rate with other cellular molecules (KFEE) were taken from Clewell et al. (2001). For KFEELU, a scaler (LLEEACT) from liver to lung used. The partition coefficients for 1-CEO were calculated with the IndusChemFate model (ver. 2.0). Simulations with the chloroprene model were carried out in R (ver. 4.0.3). The metabolite submodel model code is included in the Appendix of this supplement.

Eq 1. 1-CEO

$$\frac{d(1CEO)}{dt} = \frac{\alpha \cdot \beta \cdot VMAX \cdot CP}{Km + CP} - \frac{VMAX1O^{*} \cdot 1CEO}{KM1O + 1CEO} - \frac{VMAX1 \cdot 1CEO}{KM1 + 1CEO} - PA_{1CEO} \cdot \frac{1CEO^{**}}{P_{1CEO}}$$

Eq 2. Reactive Product

$$\frac{d(RP)}{dt} = \frac{(1-\alpha) \cdot VMAX \cdot CP}{KM + CP} - \frac{VMAX1O^{*} \cdot 1CEO}{KM1O + 1CEO} - KGSH \cdot RP \cdot GSH - KFEE \cdot RP$$

Eq 3. Glutathione (GSH)

$$\frac{d(GSH)}{dt} = K0 - \mathrm{KP} * \mathrm{GSH} - \mathrm{KGSH} \cdot RP \cdot GSH$$

* Second microsomal oxidation step in mouse liver and lung only

** For in vivo condition with transport out of tissue into blood stream

Figure F2. Rate equations for 1-CEO, reactive products (RP) and glutathione (GSH) in liver and lung.

3. RESULTS

Curves were first generated using this reactive-metabolite model to show the relationships between inhaled CP and GSH at the end of 6 hour exposures and between inhaled CP and concentrations of reactive RP and GSH at the end of 6 hours (Figure F3). The rate of metabolism versus inhaled CP follows a Michaelis-Menten form, quickly approaching a maximum rate at several 100 ppm (Figure F3 middle and bottom panel). The RPs formed by oxidation deplete GSH, with depletion to about 50% of the initial value at 15.3 ppm (Figure 3 top panel). As GSH

becomes depleted, RP cannot be cleared as efficiently and the RP concentration rise in a non-linear fashion with increasing exposure concentrations of CP.

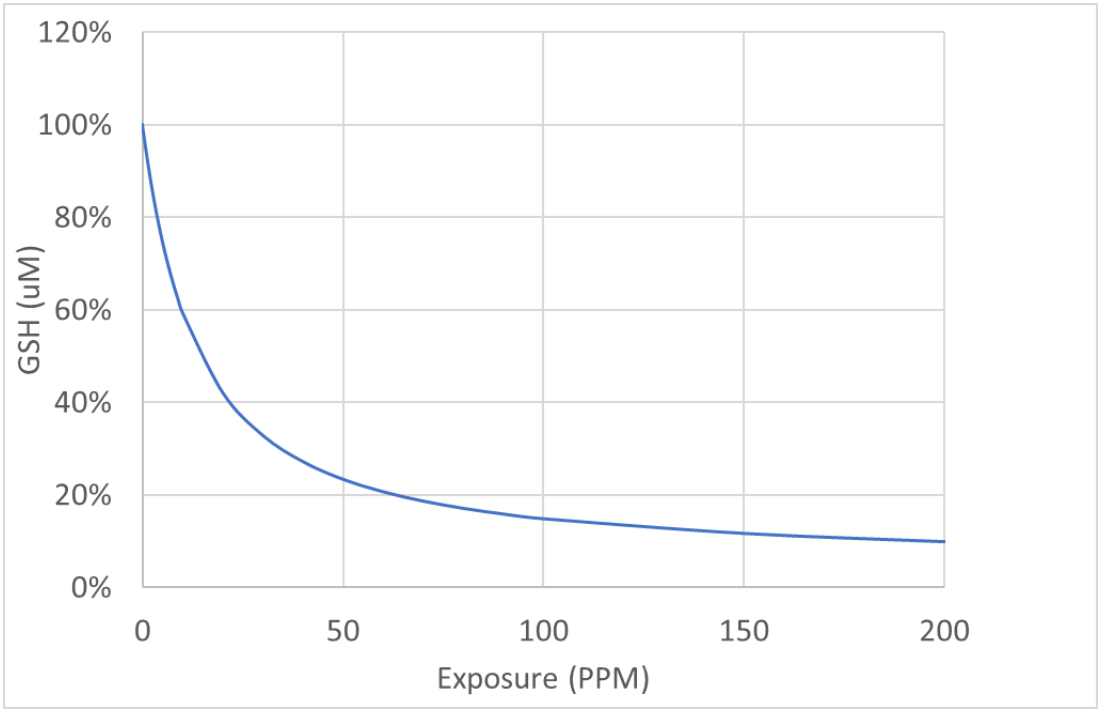

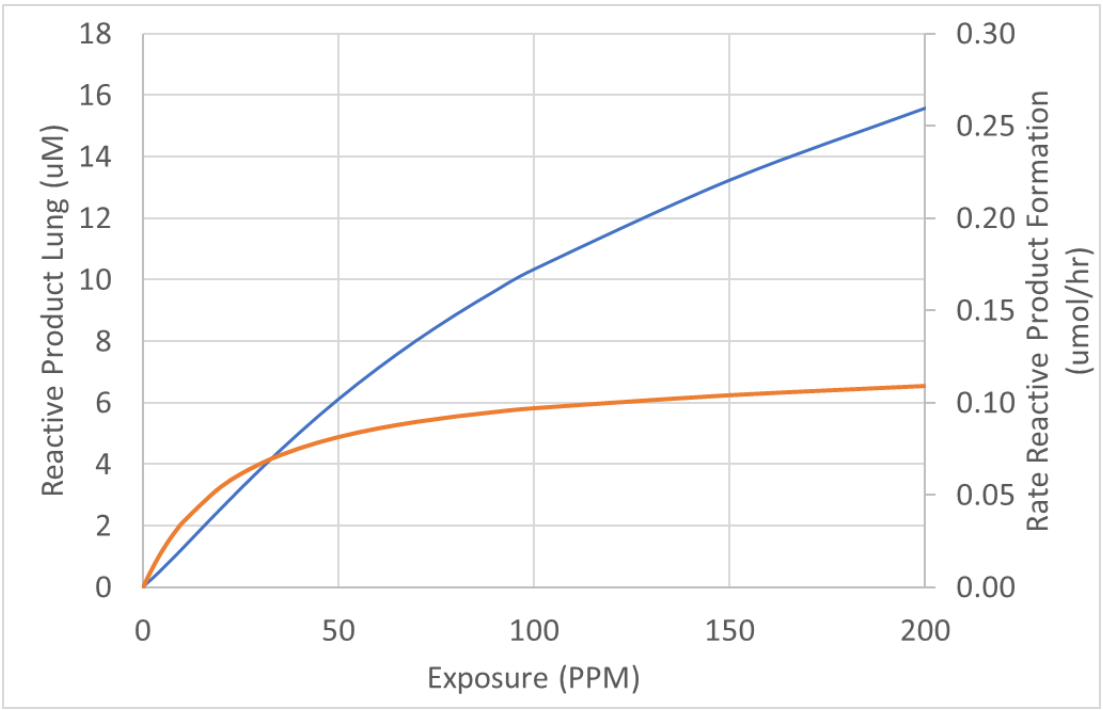

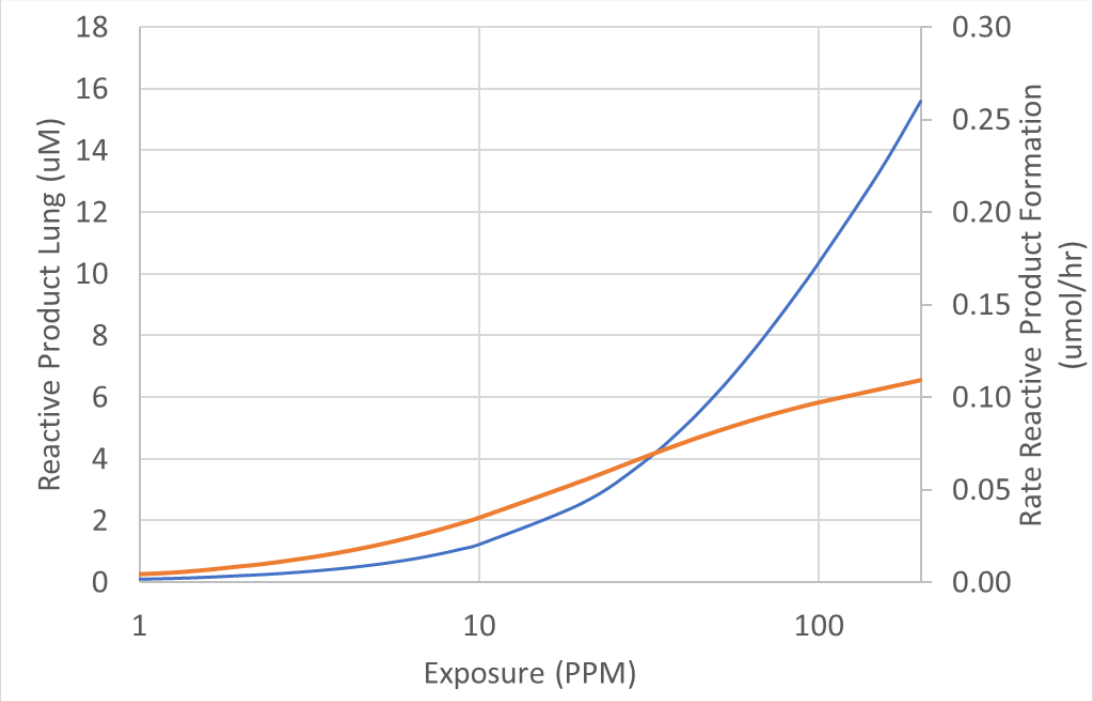

Figure F3. Predicted concentration of GSH (top panel) reactive product (middle and bottom panel, blue line) and rate of reactive product formation (middle and bottom panel, orange line) at the end of a single 6 hour exposure to chloroprene.

The extended model of chloroprene metabolism described above was exercised to evaluate three potential dose metrics for the lung toxicity and carcinogenicity of chloroprene: (1) total lung metabolism per gram lung (TMet), the dose metric used in the published PBPK models and previously submitted to the USEPA; (2) average concentration of reactive products of metabolism in the lung (PReact), and (3) average concentration of 1-CEO in the lung (1-CEO).

The first comparison performed was an evaluation of the consistency of the alternative dose metrics with the gene expression dose-response data reported in Thomas et al. (2013). In this study, female mice and rats were exposed to chloroprene by inhalation 6 hours per day, for 5 or 15 days. Mice were exposed at the bioassay concentrations, but the concentration range was extended in the rat to provide similar tissue doses based on predicted total amount of chloroprene metabolized per gram of lung tissue per day from a preliminary version of the PBPK model of Yang et al. (2012). For this comparison, two genomic responses were used: the lowest Benchmark Dose (BMD) for any gene expression change and the lowest BMD for any gene expression change related to regulation of glutathione homeostasis. A successful dose-metric for cross-species extrapolation should predict that cellular responses in the lung begin to occur at similar values of the dose metric. The results of the comparison are shown in Figure F4.

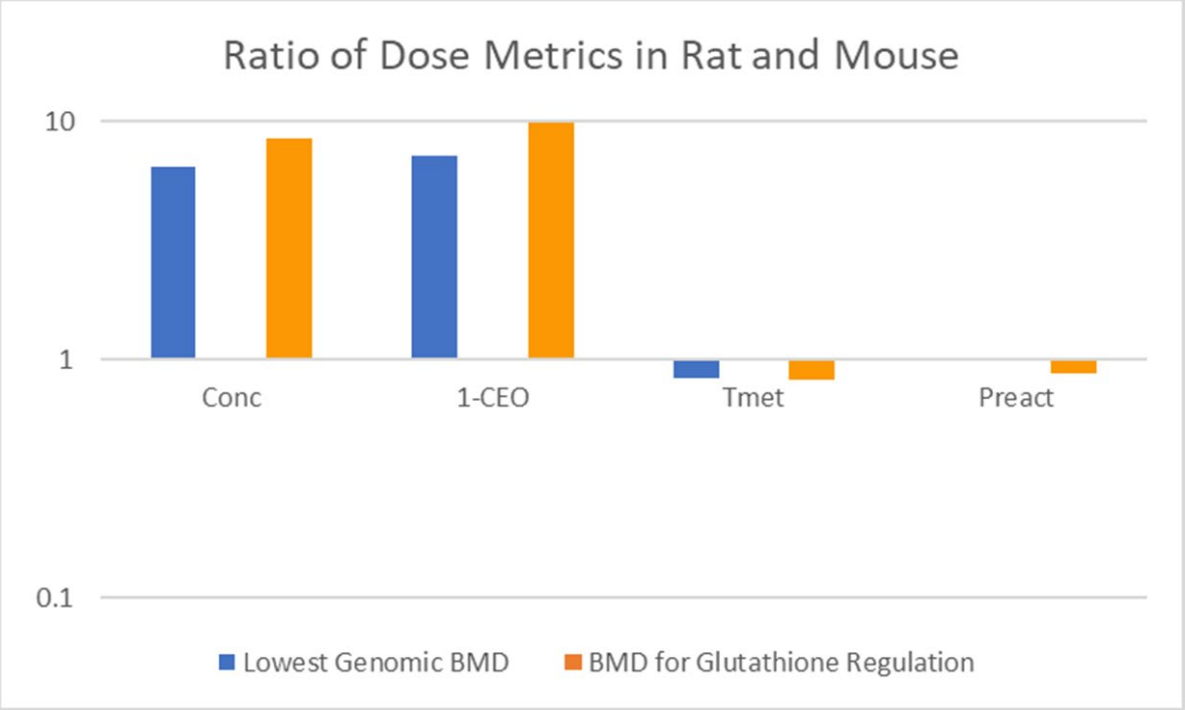

Figure F4. Cross-Species Consistency of Chloroprene Dose Metrics Based on Equivalence of Dose-Response for Gene Expression Changes (Thomas et al. 2013). An effective dose-metric for cross-species extrapolation should predict that responses in the lung occur at similar values of the dose metric, resulting in a ratio of unity. However, the lowest BMD and the lowest BMD for glutathione regulation in the rat occur at much higher inhaled concentrations (Conc) and 1-CEO concentrations (1-CEO) compared to the mouse. In contrast, they occur at similar values of total metabolism (TMet) and reactive product concentration (PReact) in the two species, supporting their appropriateness for cross-species extrapolation.

Consistent with the expectations that drove the experimental design in Thomas et al. (2013), the inhaled concentrations at which there was genomic evidence of cellular stress in the lungs of the rat were much higher than in the mouse. The predicted dose metric values for 1-CEO concentration associated with similar genomic biomarkers of cellular effects are also nearly an order of magnitude higher in the rat than in the mouse. In contrast, the model predicts similar dose metric values for both TMet and PReact in the rat and mouse, consistent with the expectation that cellular responses to chloroprene in the lung would begin to occur at similar levels of cellular stress. The consistency of these two dose metrics with the observed genomic dose-response in the female mouse and female rat, and the inconsistency of the 1-CEO or inhaled CP dose metrics, support the importance of reactive product formation in the mode of action for chloroprene.

The second comparison performed was an evaluation of the consistency of the alternative dose metrics with the tumor incidence in the bioassays for the female mouse and rat. This comparison could not be conducted in the male rat because, as described in Supplemental Materials B, the rate of metabolism in the rat lung was too low to support estimation of metabolism parameters. Figure F5(A-C) shows the predicted dose-response relationship for tumor incidence in the female mouse and female rat using the TMet, PReact and 1-CEO dose metrics. As in the previous

comparison, the TMet and Preact metrics provide a reasonable dose-response relationship with tumor incidence, whereas the 1-CEO metric does not. In fact, using the 1-CEO concentration as the dose metric would predict that the female rat should have had a higher tumor incidence than the female mouse.

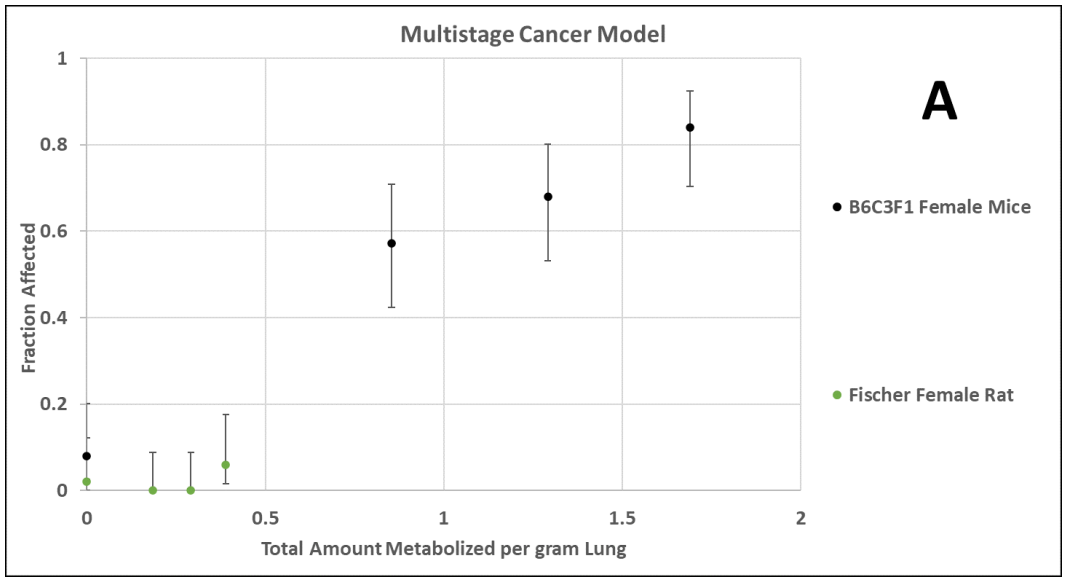

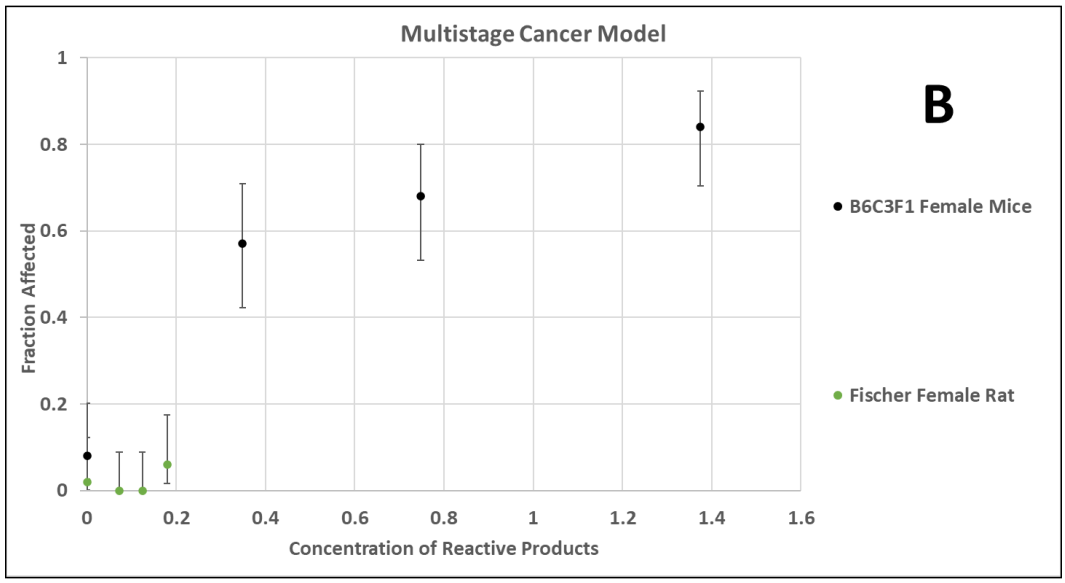

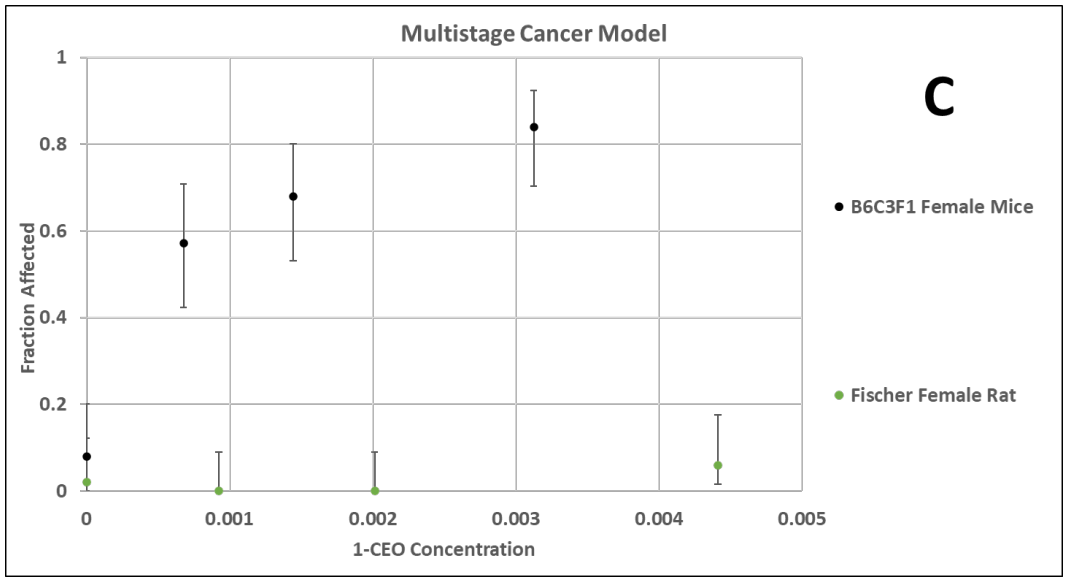

Figure F5. Benchmark dose assessment of dose metrics (A – total amount metabolized per day in lung; B – concentration of reactive products in lung; C – 1-CEO concentration in lung) predicted with the chloroprene model for the Thomas et al. 2013 concentrations.

The inconsistency of the 1-CEO dose metric with the relationships for both toxicity and carcinogenicity between the female mouse and female rat is likely due to the small proportion of total chloroprene metabolism that it represents. At the bioassay concentrations, the predicted concentrations of 1-CEO are less than 0.4% of the concentrations of reactive products in the female mouse and less than 5% in the rat.

4. DISCUSSION

Mode of Action: The toxicology and metabolism of both vinyl chloride (VC) and vinylidene chloride (VDC; 1,1-dichloroethylene) have been extremely well-characterized due to their uses as precursors for a variety of polymeric products. The research on toxicity of these compounds dates to the early 1970's. As with CP, the pathways of metabolism involve (1) CYP P450 oxidation, (2) production of reactive intermediates and (3) reaction of these reactive metabolites with glutathione and, (4), after sufficient glutathione depletion, with other cellular constituents. The reactivity toward proteins, lipids, and nucleic acids can lead to toxicity, the severity of which in turn depends on the reactivity and the dose of these metabolites. The initial studies with these two chlorinated ethylenes focused more on effects on liver rather than effects on lung, largely due to the identification of VC as a carcinogen in workers exposed to high concentrations of this monomer (Makk et al. 1974).

Cytochrome P450 mediated metabolism of VC forms an epoxide, chloroethylene oxide, which rearranges to chloroacetaldehyde. Both the epoxide and the aldehyde can react with and deplete cellular GSH (Watanabe and Gehring 1976), but even at very high inhaled concentrations, these metabolites have relatively low acute toxicity (Jaeger et al. 1974b). Both the epoxide and the aldehyde can form DNA-adducts (Green and Hathway 1978) and the tissue half-life of the epoxide will be much shorter than that of the aldehyde. Almost counter-intuitively, the carcinogenic responses to vinyl chloride arise partially due to production of metabolites that are

not themselves rapidly metabolized or overly reactive even following exposures to very high concentrations of VCM. Twenty-four hours after a 6 hr exposure to 5% VC (i.e. 50,000 ppm) there was no significant increase in alanine transaminase or sorbitol dehydrogenase in naïve rats and only a 10-to-20-fold increase in phenobarbital (PB) pretreated rats, where the PB pretreatment increases oxidative metabolism (Jaeger et al. 1974b). In the rat, the maximum metabolic rate, measured using gas uptake methods, was 40 µmoles/hr (Gargas et al. 1988) and macromolecular binding was not evident until GSH levels were decreased to 30% of basal levels (Watanabe and Gehring 1976). The cancer dose response curve was not consistent with VC as a dose metric but was consistent with the amount metabolized in the presence of significant depletion of GSH (Gehring et al. 1978; 1979), just as our extended model predicts.

Liver GSH levels are lower in fasted rats than in fed rats (Jaeger et al. 1974a). With this reduction in GSH, compounds that deplete liver GSH are more toxic to fasted than to fed rats. The LC50 of 1,1-DCE in fed rats was 15,000 ppm, but in fasted rats it was only 150 ppm. Serum enzymes increased abruptly at 100 ppm and were maximum at several hundred ppm. These responses are due to production of reactive metabolites that are cleared by GSH until the GSH becomes depleted. While the initial oxidation of 1,1-DCE produces an epoxide, this metabolite is unstable and undergoes spontaneous rearrangement producing chloroacetyl chloride, a highly reactive acid halide. These metabolites react with and deplete GSH levels. With severe GSH depletion, these metabolites react with tissue constituents leading to macromolecular binding and tissue toxicity (McKenna et al. 1977). Unlike VC, 1,1-DCE does not cause significant increases in hemangiosarcoma or any other liver tumors. However, with both VC and VDC, all metabolism goes through a single epoxide.

In early work examining the hepatic toxicity of CP in rats including the effects of fasting to restrict GSH resynthesis, Plugge and Jaeger (1979) noted that the pattern of toxicity was comparable to VDC although higher exposures of CP were required to produce equivalent increases in SAKT (Jaeger et al. 1974a; Plugge and Jaeger 1979). As noted earlier, metabolism of CP mainly produces a combination of reactive aldehydes and ketones derived from 2-(chloroethenyl)-oxirane. With only about a fraction of a*b total metabolism (3% in female mouse lung) producing 1-CEO, that itself is further oxidized to reactive products by a second oxidation in the mouse. Using kinetic constants determined for GSH synthesis and consumption from studies with styrene and styrene oxide, we showed here that the metabolism of CP in the lungs is expected to cause depletion of GSH (Figure F3 top panel) and the lung transcriptomic responses are indicative of changes in GSH metabolism as the most sensitive ontology pathway (Thomas et al. 2013). Only with sufficient GSH depletion will the reactivity with tissue components lead to extensive macromolecular binding and overt toxicity and increased tumor incidence. With VC, it was estimated that there was relatively little macromolecular binding if depletion was less than 30%. Here, our analysis showed that tumor incidence tracks with total metabolized or expected concentration of RP rather than inhaled CP or 1-CEO concentrations. All the bioassay concentrations (12.8, 30 and 80 ppm) are expected to cause much more than 30% depletion of GSH (Figure F3 top panel). Depletion of GSH to 30 % basal levels is predicted to occur at 6.8 ppm and 50% depletion at 15.3 ppm. The middle panel (Figure F3) in the plots for RP and rate of formation of RP show the non-linear relationship between RP and rate of metabolism and the increasing slope of the RP curve at low CP concentrations. Our modeling results capture the non-linear relationship between RP and total rate of metabolism. These results demonstrate the marked increase in the slope of RP as the exposure increases, and are

consistent with the body of work in the toxicology of these chlorinated compounds and on the dose response for tumors with CP.

Both 1-CEO and, (Z)-2-chlorobut-2-en-1-al, a reactive aldehyde derived from 2-CEO, formed adducts when incubated with specific nucleotides (Munter et al. 2007). While the studies are not necessarily representative of reaction conditions with native DNA in vivo, they show the ability of some 1-CEO and at least one of the reactive CP metabolites to react with bases in DNA and form adducts. Our MOA with CP does not dismiss formation of these adducts but instead highlights that there is a threshold below which macromolecular binding is small and the cancer dose response is driven by production of reactive metabolites together with increasing levels of GSH depletion. Small changes in the numbers of adducts are not expected to define the shape of the dose response curve at low doses. In fact, there is always a substantial background of various adducts with more than 40,000 altered bases per cell (Nakamura et al. 2014). At low levels of exposure, ith increases in only a small number of adducts, DNA damage response networks would still be capable of effectively maintaining the integrity of the DNA prior to cell division through non-linear feedback processes (Zhang et al. 2014; Clewell and Andersen 2016).

Overall, the dose response for lung tumors from CP is consistent with a non-linear cytotoxicity with macromolecular binding with protein, lipid and nucleic acid bases at higher exposures.

5. REFERENCES

Andersen ME, Thomas OE, Gargas ML, Jones RA, Jenkins LJ Jr. 1980. The significance of multiple detoxification pathways for reactive metabolites in the toxicity of 1,1-dichloroethylene. Toxicology and Applied Pharmacology, 52: 422-432.

Campbell J, Van Landingham C, Crowell S, Gentry R, Kaden D, Fiebelkorn S, Loccisano A, Clewell H. 2015. A preliminary regional PBPK model of lung metabolism for improving species dependent descriptions of 1,3-butadiene and its metabolites. Chemico-Biological interactions, 238: 102–110.

Clewell HJ III, Campbell JL, Van Landingham C, Franzen A, Yoon M, Dodd DE, Andersen ME, Gentry PR. 2019. Incorporation of in vitro metabolism data and physiologically based pharmacokinetic modeling in a risk assessment for chloroprene. Inhalation Toxicology, 31: 468-483.

Clewell HJ III, Campbell JL, Van Landingham C, Franzen A, Yoon M, Dodd DE, Andersen ME, Gentry PR. 2020. Response to "letter concerning: Clewell (2019) incorporation of in vitro metabolism data and physiologically based pharmacokinetic modeling in a risk assessment for chloroprene." (UIHT-2020-0053). Inhalation Toxicology, 32: 369-371.

Clewell HJ III, Gentry PR, Gearhart JM, Allen BC, Andersen ME. 2001. Comparison of cancer risk estimates for vinyl chloride using animal and human data with a PBPK model. The Scienc of the Total Environment, 274: 37-66.

Clewell RA, Andersen ME. 2016. Approaches for characterizing threshold dose-response relationships for DNA-damage pathways involved in carcinogenicity in vivo and micronuclei formation in vitro. Mutagenesis, 31: 333-340.

Cottrell L, Golding BT, Munter T, Watson WP. 2001. In vitro metabolism of chloroprene: species differences, epoxide stereochemistry and a de-chlorination pathway. Chemical Research in Toxicology, 14: 1552-1562.

Csanady GA, Kessler W, Hoffmann HD, Filser JG. 2003. A toxicokinetic model for styrene and its metabolite styrene-7,8-oxide in mouse, rat and human with special emphasis on the lung. Toxicology Letters, 138: 75-102.

D'Souza RW, Andersen ME. 1988. Physiologically based pharmacokinetic model for vinylidene chloride. Toxicology and Applied Pharmacology, 95: 230-240.

D'Souza RW, Francis WR, Andersen ME. 1988. Physiological model for tissue glutathione depletion and increased resynthesis after ethylene dichloride exposure. Journal of Pharmacology and Experimental Therapeutics, 245: 563-568.

ENVIRON International. 2004. Application of a PBPK Model for Cancer and Noncancer Risk Assessment of 1,2-Dichloroethane. Phase II: Modifications to the PBPK Model for DCE and its Application in the Estimation of Dose Metrics for Risk Assessment. Requistion/Reference No. 2W2E59, QT-DC-03-000387.

Filser JG, Klein D. 2018. A physiologically based toxicokinetic model for inhaled ethylene and ethylene oxide in mouse, rat, and human. Toxicology Letters, 286: 54-79.

Gargas ML, Seybold PG, Andersen ME. 1988. Modeling the tissue solubilities and metabolic rate constant (Vmax) of halogenated methanes, ethanes, and ethylenes. Toxicology Letters, 43: 235-256.

Gehring PJ, Watanabe PG, Park CN. 1978. Resolution of dose-response toxicity data for chemicals requiring metabolic activation: example--vinyl chloride. Toxicology and Applied Pharmacology, 44: 581-591.

Gehring PJ, Watanabe PG, Park CN. 1979. Risk of angiosarcoma in workers exposed to vinyl chloride as predicted from studies in rats. Toxicology and Applied Pharmacology, 49: 15-21.

Green T, Hathway DE. 1978. Interactions of vinyl chloride with rat-liver DNA in vivo. Chemico-Biological Interactions, 22: 211-224.

Himmelstein MW, Carpenter SC, Hinderliter PM. 2004. Kinetic modeling of beta-chloroprene metabolism: I. In vitro rates in liver and lung tissue fractions from mice, rats, hamsters, and humans. Toxicological Sciences, 79: 18-27.

Jaeger RJ, Conolly RB, Murphy SD. 1974a. Effect of 18 hr fast and glutathione depletion on 1,1-dichloroethylene-induced hepatotoxicity and lethality in rats. Experimental and Molecular Pathology, 20: 187-198.

Jaeger RJ, Conolly RB, Reynolds ES, Murphy SD. 1975. Biochemical toxicology of unsaturated halogenated monomers. Environmental Health Perspectives, 11: 121-128.

Jaeger RJ, Reynolds ES, Conolly RB, Moslen MT, Szabo S, Murphy SD. 1974b. Acute hepatic injury by vinyl chloride in rats pretreated with phenobarbital. Nature, 252: 724-726.

Johanson G, Filser JG. 1993. A physiologically based pharmacokinetic model for butadiene and its metabolite butadiene monoxide in rat and mouse and its significance for risk extrapolation. Archives in Toxicology, 67: 151-163.

Kohn MC, Melnick RL. 2000. The privileged access model of 1,3-butadiene disposition. Environmental Health Perspectives, 108(Suppl 5): 911-917.

Makk L, Creech JL, Whelan JG Jr, Johnson MN. 1974. Liver damage and angiosarcoma in vinyl chloride workers. A systematic detection program. JAMA, 230: 64-68.

McKenna MJ, Watanabe PG, Gehring PJ. 1977. Pharmacokinetics of vinylidene chloride in the rat. Environmental Health Perspectives, 21: 99-105.

Munter T, Cottrell L, Ghai R, Golding BT, Watson WP. 2007. The metabolism and molecular toxicology of chloroprene. Chemico-Biological Interactions, 166: 323-331.

Munter T, Cottrell L, Golding BT, Watson WP. 2003. Detoxication pathways involving glutathione and epoxide hydrolase in the in vitro metabolism of chloroprene. Chemical Research in Toxicology, 16: 1287-1297.

Nakamura J, Mutlu E, Sharma V, Collins L, Bodnar W, Yu R, Lai Y, Moeller B, Lu K, Swenberg J. 2014. The endogenous exposome. DNA Repair (Amst), 19: 3-13.

Plugge H, Jaeger RJ. 1979. Acute inhalation toxicity of 2-chloro-1,3-butadiene (chloroprene): effects on liver and lung. Toxicology and Applied Pharmacology, 50: 565-572.

Thomas RS, Himmelstein MW, Clewell HJ III, Yang Y, Healy E, Black MB, Andersen ME. 2013. Cross-species transcriptomic analysis of mouse and rat lung exposed to chloroprene. Toxicological Sciences, 131: 629-640.

Watanabe PG, Gehring PJ. 1976. Dose-dependent fate of vinyl chloride and its possible relationship to oncogenicity in rats. Environmental Health Perspectives, 17: 145-152.

Yang Y, Himmelstein MW, Clewell HJ III. 2012. Kinetic modeling of b-chloroprene metabolism: Probabilistic *in vitro–in vivo* extrapolation of metabolism in the lung, liver and kidneys of mice, rats and humans. Toxicology *in Vitro,* 26(6): 1047–1055.

Zhang Q, Bhattacharya S, Conolly RB, Clewell HJ III, Kaminski NE, Andersen ME. 2014. Molecular signaling network motifs provide a mechanistic basis for cellular threshold responses. Environmental Health Perspectives, 122: 1261-1270.

APPENDIX 1

Chloroprene model code for the epoxy submodel
#Chloroprene PBPK Model
#Translated from the acslX model presented in Yang et al. 2012
#By Jerry Campbell 2019
#Added Tracheobronchial region
#Added 1-CEO, Reaction Product and GSH submodels
#By Jerry Campbell 2021

```
States  = {
AI ,
AX ,
AM ,
AMCP_1CE ,
AMCP_2CE ,
AMLU ,
AMLUCP_1CE ,
AMLUCP_2CE ,
AMK ,
ALU ,
AL ,
AK ,
AS ,
AR ,
AUCCR ,
AF ,
AX1 ,
AM1 ,
AMLU1 ,
AM1O ,
AMLU1O  ,
ALUE1 ,
ALU1 ,
ALE1 ,
AL1 ,
AS1 ,
AR1 ,
AF1          ,
ARPG         ,
ARPGLU       ,
ARPEE        ,
ARPEELU      ,
ALRPPRO ,
ALRP         ,
ALURPPRO ,
ALURP        ,
AGSHL        ,
AGSHLU       ,
```

```
AUCCLRP      ,
AUCCLURP     ,
AUCCEO1L  ,
AUCCEO1LU ,
AUCGSHL ,
AUCGSHLU
};

Outputs = {
CVL ,
GSHL ,
GSHLU ,
CLRP  ,
CLURP ,
VL  ,
MASBAL ,
A1CEOGEN ,
MASBAL1 ,
CLU          ,
CL           ,
CK           ,
CS           ,
CR           ,
CF           ,
CV  ,
CVLUM        ,
CVLUM1 ,
CLUE1 ,
CLU1  ,
CLE1 ,
CL1          ,
CS1          ,
CR1          ,
CF1          ,
CV1  ,
qcbal ,
vbal ,
ppm ,
AMP          ,
AMPLU        ,
AMPK         ,
AM1L ,
AM1LU ,
AM1LO ,
AM1LUO ,
ARPL  ,
ARPLU ,
```

```
ARPOTHL ,
ARPOTHLU ,
ARPGSHL ,
ARPGSHLU ,
CLRPAVG ,
CLURPAVG ,
CL1AVG  ,
CLU1AVG ,
GSHLAVG ,
GSHLUAVG
};



Inputs = {EXPPULSE}  ;


#BODY WEIGHT (kg)
BW = 0.03 ;    # Body weight (kg)


#SPECIAL FLOW RATES
QPC = 29.1 ;     # Unscaled Alveolar Vent (L/h/kg^0.75)
QCC = 20.1 ;     # Unscaled Cardiac Output (L/h/kg^0.75)

#FRACTIONAL BLOOD FLOWS TO TISSUES
QLC = 0.161 ;   # Flow to Liver as % Cardiac Output (unitless)
QFC = 0.07  ;   # Flow to Fat as % Cardiac Output (unitless)
QSC = 0.159 ;   # Flow to Slow as % Cardiac Output (unitless)
QKC = 0.09  ;   # Flow to Kidney as % Cardiac Output (unitless)


#FRACTIONAL VOLUMES OF TISSUES
VLC = 0.055 ;      # Volume Liver as % Body Weight (unitless)
VLUC = 0.0073 ;   # Volume Lung as % Body Weight (unitless)
VFC = 0.1  ;         # Volume Fat as % Body Weight (unitless)
VRC = 0.08098 ;      # Volume Rapid Perfused as % Body Weight (unitless)
VSC = 0.384  ;       # Volume Slow Perfused as % Body Weight (unitless)
VKC = 0.0167 ;      # Volume Kidney as % Body Weight  (unitless)

#PARTITION COEFFICIENTS PARENT
#Chloroprene
PL = 1.26 ;    # Liver/Blood Partition Coefficient (unitless)
PLU = 2.38 ;    # Lung/Blood Partition Coefficient (unitless)
PF = 17.35 ;    # Fat/Blood Partition Coefficient (unitless)
PS = 0.59  ;   # Slow/Blood Partition Coefficient (unitless)
PR = 1.76 ;    # Rapid/Blood Partition Coefficient (unitless)
```

```
PB = 7.83 ;    # Blood/Air Partition Coefficient (unitless)
PK = 1.76 ;    # Kidney/Blood Partition Coefficient (unitless)

#PARTITION COEFFICIENTS 1-CEO (IndusChemFate, LogKow 1.22)
PL1 = 1.26 ;     # Liver/Blood Partition Coefficient (unitless)
PLU1 = 2.38 ;    # Lung/Blood Partition Coefficient (unitless)
PF1 = 17.35 ;    # Fat/Blood Partition Coefficient (unitless)
PS1 = 0.59  ;    # Slow/Blood Partition Coefficient (unitless)
PR1 = 1.76 ;     # Rapid/Blood Partition Coefficient (unitless)
PB1 = 7.8 ;     # Blood/Air Partition Coefficient (unitless)



#KINETIC CONSTANTS
MW = 88.5  ;   # Molecular weight (g/mol)
MWCEO = 104.5 ;  # 1-CEO Molecular weight (g/mol)

#Chloroprene
#Fraction of total metabolism to 1-CEO
ALPHAL = 0.02 ;   #Fraction of liver chloroprene metabolism to 1-CEO
ALPHALU = 0.03 ;   #Fraction of lung chloroprene metabolism to 1-CEO
#Fraction of total CP to 1-CEO privaleged access
#(based on butadiene model Campbell et al. 2015; assumed same in liver and lung)
BETA = 0.67 ;

# CP Metabolism in Liver
VMAXC = 7.95  ;   # Scaled VMax for Oxidative Pathway:Liver (mg/h/BW^0.75)
KM = 0.041  ;   # Km for Oxidative Pathway:Liver (mg/L)

# CP Metabolism in Lung
VMAXCLU = 0.18;     # Scaled VMax for Oxidative Pathway:Lung (mg/h/BW^0.75)
KMLU = 0.26;        # Km for Oxidative Pathway:Lung (mg/L)

# CP Metabolism in Kidney
VMAXCKid = 0.0 ;    # Scaled VMax for Oxidative Pathway:Kidney (mg/h/BW^0.75)
KMKD = 1.0  ;   # Km for Oxidative Pathway :Kidney

#1-CEO
#1-CEO Metabolism in Liver - Hydrolysis
VMAXC1 = 7.95  ;   # Scaled VMax for Hydrolysis Pathway:Liver (mg/h/BW^0.75)
KM1 = 0.041  ;   # Km for Hydrolysis Pathway:Liver (mg/L)

#1-CEO Metabolism in Lung - Hydrolysis
VMAXCLU1 = 0.18;     # Scaled VMax for Hydrolysis Pathway:Lung (mg/h/BW^0.75)
KMLU1 = 0.26;        # Km for Hydrolysis Pathway:Lung (mg/L)

#1-CEO Metabolism in Liver - Oxidative (Mouse Only!!!)
```

```
VMAXC1O = 7.95  ;   # Scaled VMax for Oxidative Pathway:Liver (mg/h/BW^0.75)
KM1O = 0.041  ;   # Km for Oxidative Pathway:Liver (mg/L)


#Reactive Products
#Liver
KGSHLC = 0.0 ;     #2nd order rate of RP reaction with GSH
K3L = 0.0 ;     #Reaction rate with cellular macromolecules
MML = 0.0 ;     #macrolecule concentration (mM)


#Lung
KGSHLUC = 0.0 ;     #2nd order rate of RP reaction with GSH (L/mmol/hr)
K3LU = 0.0 ;     #Reaction rate with cellular macromolecules (L/mmol/hr)
MMLU = 0.0 ;   #macrolecule concentration (mM)

#GSH
K0L = 0.0 ;         #Production of GSH
K1L = 0.0 ;         #Background loss of GSH

K0LU = 0.0 ;         #Production of GSH
K1LU = 0.0 ;         #Background loss of GSH

#Permeation Coefficient (fraction of blood flow)
PA1 = 1.0 ;        #Permeation Coefficient for 1-CEO in lung

#DOSING INFORMATION
TSTOP = 7.0 ;     # Dosing stop time
CONC = 13.0  ;   # Initial concentration (ppm)

#Parameters for GSH submodel
LLOXACT = 0.14 ;    #Scaler for liver to lung oxidative metabolism 1-CEO (mouse only)
LLEEACT = 0.06 ;    #Scaler for liver to lung oxidative metabolism 1-CEO (mouse only)

KFEEC = 4500.0 ;    # 1/hr/kg Conjugation rate with non-GSH
  KPC = 0.06  ;     # First-order rate constant for GSH loss
  GSO = 5500.0  ;   # Initial GSH concentration liver
GSOLU = 1200.0  ;   # Initial GSH concentration lung



Dynamics {
#########################################################################
######################
# Scaled parameters

      QC = QCC*pow(BW,0.75)  ;       #Cardiac output
```

```
      QP = QPC*pow(BW,0.75)  ;       #Alveolar ventilation
      QL = QLC*QC    ;              #Liver blood flow
      QF = QFC*QC    ;              #Fat blood flow
      QS = QSC*QC    ;              #Slowly-perf tissue blood flow
      QK = QKC*QC    ;              #Kidney tissue blood flow

     QRC = 1 - QLC - QKC - QFC - QSC ;  #Rapily Perfused tissues
      QR = QRC*QC            ;                          #Rapily-perf tissue blood flow

      VL = VLC*BW      ;           #Liver volume
     VLU = VLUC*BW     ;            #Lung volume
      VF = VFC*BW      ;           #Fat tissue volume
      VS = VSC*BW      ;           #Slowly-perfused tissue volume
      VR = VRC*BW      ;           #Richly-perfised tissue volume
      VK = VKC*BW      ;           #kidney tissue volume

   ROBC = 1 - VLC - VLUC - VFC - VSC - VRC - VKC ;  #Rest of body un-perfused tissue for MC

# METABOLISM
    VMAX = VMAXC*pow(BW,0.75)  ;       #Maximum rate of metabolism-Liver (mg/hr)
  VMAXLU = VMAXCLU*pow(BW,0.75) ;       #Maximum rate of metabolism-Lung (mg/hr)
  VMAXKD = VMAXCKid*pow(BW,0.75)  ;     #Maximum rate of metabolism-Kidney (mg/hr)

   VMAX1 = VMAXC1*pow(BW,0.75)  ;      #Maximum rate of metabolism-Liver (mg/hr)
 VMAXLU1 = VMAXCLU1*pow(BW,0.75) ;      #Maximum rate of metabolism-Lung (mg/hr)
  VMAX1O = VMAXC1O*pow(BW,0.75)  ;      #Maximum rate of metabolism-Liver (mg/hr)

  VMAXLU1O = VMAX1O*LLOXACT ;          #Liver Vmax scaled to lung (ECD model)

   KGSHL = KGSHLC;
    KFEE = KFEEC ;
  KGSHLU = KGSHLUC;
  KFEELU = KFEE*LLEEACT  ;
     KP = KPC*pow(BW,-0.3)  ;
   KOTDL = KP*GSO ;
 KOLUTDL = KP*GSOLU ;



#############################################################
######################
# Exposure Control (mg/L)
     CIX = CONC*MW/24450 ;
      CI = CIX *EXPPULSE  ;

#############################################################
######################
```

```
# Chloroprene
# Tissue Venous Concentrations (mg/L)
    CVLU = ALU/(VLU*PLU) ;
     CVL = AL/(VL*PL) ;
     CVK = AK/(VK*PK) ;
     CVS = AS/(VS*PS) ;
     CVR = AR/(VR*PR) ;
     CVF = AF/(VF*PF) ;

#Tissue Concentration (mg/L)
# 1-CEO
# Tissue Venous Concentrations (mg/L)
     CLUE1 = ALUE1/VLU ;
     CVLU1 = ALU1/(VLU*PLU1) ;
     CLU1  = (ALUE1+ALU1)/VLU ;
     CLE1  = ALE1/VL ;
     CVL1  = AL1/(VL*PL1) ;
     CL1   = (ALE1 + AL1)/VL ;
     CVS1  = AS1/(VS*PS1) ;
     CVR1  = AR1/(VR*PR1) ;
     CVF1  = AF1/(VF*PF1) ;


#Concentration of GSH in Liver and Lung
  GSHL = AGSHL/VL ;     #GSH concentraiton in liver (mM)
  GSHLU = AGSHLU/VLU ;  #GSH concentraiton in lung (mM)



#############################################################
######################
# Concentration in Pulmonary/Arterial and venous blood Compartments (mg/L)
     CPU = (QP*CI+(QF*CVF + QL*CVL + QS*CVS + QR*CVR + QK*CVK))/(QP/PB+QC)  ;
      CX = CPU/PB ;
      CV = (QF*CVF + QL*CVL + QS*CVS + QR*CVR + QK*CVK)/QC ;
    CPUM = CPU*1000/MW ;
     RAI = QP*CI ;
     dt(AI) = RAI ;
     RAX = QP*CX ;
     dt(AX) = RAX ;

#############################################################
######################
#############################################################
######################
#Rate amount metabolized in liver, lung and kidney
```

```
# Amount metabolized in Liver (mg)
    RAM = VMAX*CVL/(KM+CVL) ;
    dt(AM) = RAM ;

    #Total 1 and 2-CEO from CP
    RAMCP_1CEO = RAM*ALPHAL ;    #CP metabolized to 1-CEO in Liver
    dt(AMCP_1CE) = RAMCP_1CEO ;

    RAMCP_2CEO = RAM*(1-ALPHAL) ; #CP metabolized to 2-CEO in Liver
    dt(AMCP_2CE) = RAMCP_2CEO ;


# Amount metabolized in Lung (mg)
    RAMLU = VMAXLU*CVLU/(KMLU+CVLU) ;
    dt(AMLU) = RAMLU ;

    RAMLUCP_1CEO = RAMLU*ALPHALU ; #CP metabolized to 1-CEO in Lung
    dt(AMLUCP_1CE) = RAMLUCP_1CEO ;

    RAMLUCP_2CEO = RAMLU*(1-ALPHALU) ; #CP metabolized to 2-CEO in Lung
    dt(AMLUCP_2CE) = RAMLUCP_2CEO ;

# Amount metabolized in Kidney (mg)
    RAMK = VMAXKD*CVK/(KMKD + CVK)  ;
    dt(AMK) = RAMK ;

#############################################################
######################
#############################################################
######################

# Amount in Lung Compartment (mg)
    RALU = QC*(CPU-CVLU) - RAMLU  ;
    dt(ALU) = RALU ;

# Amount in Liver Compartment (mg)
    RAL = QL*(CVLU-CVL) - RAM ;
    dt(AL) = RAL ;

# Amount in Kidney Compartment (mg)
    RAK = QK*(CVLU-CVK) - RAMK ;
    dt(AK) = RAK ;

# Amount in Slowly Perfused Tissues (mg)
    RAS = QS*(CVLU-CVS) ;
    dt(AS) = RAS ;
```

```
# Amount in Rapidly Perfused Tissues (mg)
     RAR = QR*(CVLU-CVR) ;
     dt(AR) = RAR ;
     dt(AUCCR) = AR/VR ;

# Amount in Fat Compartment (mg)
     RAF = QF*(CVLU-CVF) ;
     dt(AF) = RAF ;

############################################################################
#############
############################################################################
#############

#1-CEO submodel

############################################################################
######################
############################################################################
######################
############################################################################
######################
# Concentration 1-CEO in Pulmonary/Arterial and venous blood Compartments (mg/L)
      CV1 = (QF*CVF1 + QL*CVL1 + QS*CVS1 + (QR+QK)*CVR1)/QC ;
     CPU1 = (QC*CV1)/(QP/PB1+QC)  ;
      CX1 = CPU1/PB1 ;
     RAX1 = QP*CX1 ;
   dt(AX1) = RAX1 ;

#Rate amount 1-CEO metabolized in liver and lung
#Hydrolysis (1-CEO to diol)
# Amount metabolized in Liver (mg)
       RAM1 = VMAX1*CVL1/(KM1 + CVL1) ;
    dt(AM1) = RAM1 ;

# Amount metabolized in Lung (mg)
     RAMLU1 = VMAXLU1*CVLU1/(KMLU1 + CVLU1) ;
   dt(AMLU1) = RAMLU1 ;

#Oxidative (Mouse Only!!!)
# Amount metabolized in Liver (mg)
       RAM1O = VMAX1O*CVL1/(KM1O + CVL1) ;
    dt(AM1O) = RAM1O ;

# Amount metabolized in Lung (mg)
       RAMLU1O = VMAXLU1O*CVLU1/(KM1O + CVLU1) ;
    dt(AMLU1O) = RAMLU1O ;
```

```
#############################################################################
#######################
#############################################################################
#######################

# 1-CEO in Lung Compartment
# Amount in Lung Epithelium (mg)
    RALUE1 = PA1*QC*(CVLU1 - CLUE1/PLU1) + RAMLUCP_1CEO*BETA*MWCEO/MW - RAMLU1
- RAMLU1O ;
    dt(ALUE1) = RALUE1 ;

# Amount in Lung Submucosa (mg)
    RALU1 = QC*(CPU1-CVLU1) + PA1*QC*(CLUE1/PLU1 - CVLU1) ;
    dt(ALU1) = RALU1 ;

# 1-CEO in Liver
# Amount in Liver Epithelium (mg)
    RALE1 = PA1*QL*(CVL1 - CLE1/PL1) + RAMCP_1CEO*BETA*MWCEO/MW - RAM1 - RAM1O ;
    dt(ALE1) = RALE1 ;

# Amount in Liver Compartment (mg)
    RAL1 = QL*(CVLU1-CVL1) + PA1*QL*(CLE1/PL1 - CVL1) ;
    dt(AL1) = RAL1 ;


# Amount in Slowly Perfused Tissues (mg)
    RAS1 = QS*(CVLU1 - CVS1) ;
    dt(AS1) = RAS1 ;

# Amount in Rapidly Perfused Tissues (mg)
    RAR1 =(QR+QK)*(CVLU1 - CVR1) ;
    dt(AR1) = RAR1 ;

# Amount in Fat Compartment (mg)
    RAF1 = QF*(CVLU1 - CVF1) ;
    dt(AF1) = RAF1 ;

#############################################################################
#############
#############################################################################
#############
#############################################################################
#############

#Reactive Products (converted to umol or umol/L for GSH submodel)
```

```
#############################################################################
#######################
#############################################################################
#######################

 CLRP = ALRP/VL ;    #(umol/L)
CLURP = ALURP/VLU ;    #(umol/L)


# ACMG = AMOUNT METABOLITE CONJUGATED WITH GLUTATHIONE (UMOLES)
     RARPG = KGSHL*GSHL*CLRP*VL ;
  dt(ARPG) = RARPG ;

   RARPGLU = KGSHLU*GSHLU*CLURP*VLU ;
dt(ARPGLU) = RARPGLU ;

# ACMEE = AMOUNT METABOLITE CONJUGATED WITH OTHER THINGS (UMOLES)
    RARPEE = KFEE*CLRP*VL ;
 dt(ARPEE) = RARPEE ;

  RARPEELU = KFEELU*CLURP*VLU ;
dt(ARPEELU) = RARPEELU  ;


 #Reactive products in liver (umol)
dt(ALRPPRO) = (RAMCP_2CEO/MW)*1000 + (RAM1O/MWCEO)*1000 ;
     RALRP =  (RAMCP_2CEO/MW)*1000 + (RAM1O/MWCEO)*1000 - RARPG - RARPEE ;
  dt(ALRP) = RALRP ;

 #Reactive products in lung (umol)
dt(ALURPPRO) = (RAMLUCP_2CEO/MW)*1000 + (RAMLU1O/MWCEO)*1000 ;
    RALURP = (RAMLUCP_2CEO/MW)*1000 + (RAMLU1O/MWCEO)*1000 - RARPGLU - RARPEELU
;
 dt(ALURP) = RALURP ;


#############################################################################
#############
#############################################################################
#############

#GSH

#############################################################################
#######################
```

```
#############################################################################
#######################

  #GSH in liver (umol)
    RAGSHL = KOTDL*VL - KP*GSHL*VL - RARPG  ;
 dt(AGSHL) = RAGSHL ;

  #GSH in LU (umol)
    RAGSHLU = KOLUTDL*VLU - KP*GSHLU*VLU - RARPGLU  ;
 dt(AGSHLU) = RAGSHLU ;

#AUCs for reactive products and 1-CEO:
dt(AUCCLRP) = CLRP ;  #uM*hr
dt(AUCCLURP) = CLURP ;  #uM*hr
dt(AUCCEO1L) = CL1/MWCEO*1000 ;  #uM*hr
dt(AUCCEO1LU) = CLU1/MWCEO*1000 ;  #uM*hr

dt(AUCGSHL) = GSHL ;  #uM*hr
dt(AUCGSHLU) = GSHLU ;  #uM*hr

#############################################################################
#######################
#############################################################################
#######################
#############################################################################
#######################

} # End of Dynamics

#############################################################################
#############
#############################################################################
#############
#############################################################################
#############
CalcOutputs {
# Mass-balance
               MASBAL  = AI - AX - (AL+AM+AMLU+AK+AMK+AS+AR+AF+ALU) ;
               A1CEOGEN = AM*ALPHAL*(1-BETA)*MWCEO/MW + AMLU*ALPHALU*(1-
BETA)*MWCEO/MW ;
               MASBAL1 =  A1CEOGEN - AX1 - (AM1+AMLU1+AM1O+AL1+AS1+AR1+AF1+ALU1)
;

               #Tissue Concentrations (mg/L)
       CLU = ALU/VLU ;
        CL = AL/VL ;
        CK = AK/VK ;
```

```
        CS = AS/VS ;
        CR = AR/VR ;
        CF = AF/VF ;
#Concentrations for plots
                CVLUM = CV*1000/MW ;  #(umol/L)
 CVLUM1 = CV1*1000/MWCEO ;  #(umol/L)

                #Tissue Concentrations 1-CEO (mg/L)
        CS1 = AS1/VS ;
        CR1 = AR1/VR ;
        CF1 = AF1/VF ;

#Blood Flow balance
  qcbal = QC - QL - QF - QS - QK - QR ;
#Tissue Volume balance
   vbal = BW*(1-ROBC) - VL - VLU - VF - VS - VK - VR ;

#Dose metrics are only correct when simulation time=tstop
  ppm = CONC ;

   #Total Metabolism umol/g/day
  AMP = ((AM*1000/MW)/(VL*1000))/(TSTOP/24) ;
 AMPLU = ((AMLU*1000/MW)/(VLU*1000))/(TSTOP/24) ;
 AMPK = ((AMK*1000/MW)/(VK*1000))/(TSTOP/24) ;

 #Hydrolase Metabolism of 1-CEO (umol/g/day)
 AM1L = ((AM1)/(VL*1000))/(TSTOP/24) ;
AM1LU = ((AMLU1)/(VLU*1000))/(TSTOP/24) ;

 #Oxidative metabolims of 1-CEO umol/g/day
 AM1LO = ((AM1O)/(VL*1000))/(TSTOP/24) ;
 AM1LUO = ((AMLU1O)/(VLU*1000))/(TSTOP/24) ;

 #Total production of RP (umol/g/day)
 ARPL = ((ALRPPRO)/(VL*1000))/(TSTOP/24) ;
ARPLU = ((ALURPPRO)/(VLU*1000))/(TSTOP/24) ;

 #Total reaction of RP with other (umol/g/day)
 ARPOTHL = ((ARPEE)/(VL*1000))/(TSTOP/24) ;
ARPOTHLU = ((ARPEELU)/(VLU*1000))/(TSTOP/24) ;

 #Total reaction of RP with GSH (umol/g/day)
 ARPGSHL = ((ARPG)/(VL*1000))/(TSTOP/24) ;
ARPGSHLU = ((ARPGLU)/(VLU*1000))/(TSTOP/24) ;

#Average concentration of RP (uM)
CLRPAVG = AUCCLRP/TSTOP ;
```

```
 CLURPAVG = AUCCLURP/TSTOP ;

 #Average concentration of 1-CEO (uM)
 CL1AVG = AUCCEO1L/TSTOP ;
 CLU1AVG = AUCCEO1LU/TSTOP ;

 #Average concentration of GSH (uM)
 GSHLAVG = AUCGSHL/TSTOP ;
 GSHLUAVG = AUCGSHLU/TSTOP ;


} # End of CalcOutputs

End.
```